RSC Advances

ROYAL SOCIETY OF CHEMISTRY

www.rsc.org/advances

Graphical Abstract

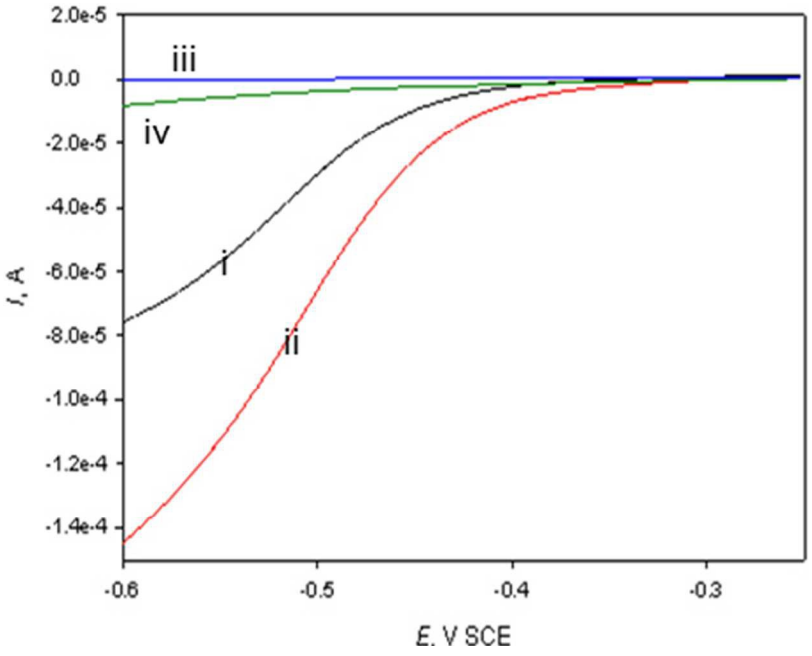

Linear Sweep Voltammograms (LSVs) at a scan rate of 50 mV s^{-1} shows the enhanced electrocatalytic properties of the hydrogen-reduced graphene oxide/TiO_2 composite compared to the GC electrode in (i & ii) oxygen and (iii & iv) argon-saturated 0.5 M H_2SO_4 at 25 °C in the presence (ii & iv) and absence (i & iii) of 300 Watt UV radiation.

Journal Name

ARTICLE

Effect of Graphene Oxide Reduction Method on the Photocatalytic and Electrocatalytic Activities of Reduced Graphene Oxide/TiO_2 Composite

Received 00th January 20xx,
Accepted 00th January 20xx

DOI: 10.1039/x0xx00000x

www.rsc.org/

H. Al-Kandari,[a] A. M. Abdullah,[b, †] S. Al-Kandari,[c] A. M. Mohamed[c]

Graphene oxide (GO) was synthesized from commercial graphite using a modified Hummers' method. Three different methods were used to prepare GO/TiO_2 composites. GO was (i) initially impregnated over TiO_2 (GOTi) and then reduced using a stream of hydrogen gas at 450 °C (H_2RGOTi), (ii) reduced using hydrazine hydrate solution (HH) in a 1000-W microwave oven (HHRGO) and then loaded on the TiO_2 (HHRGOTi) or (iii) hydrothermally reduced (RGO) then loaded on TiO_2 (RGOTi). Different characterization techniques were used e.g. X-ray photoelectron spectroscopy (XPS), X-ray diffraction patterns (XRD) and UV-Vis, Fourier transform infrared (FT-IR) and Raman Spectroscopy. The effect of the GO reduction method on the photocatalytic activity of the aforementioned composites towards the degradation of phenol in the presence and absence of (i) UV and (ii) H_2O_2 was examined. High phenol degradation rates were achieved using the RGOTi photocatalyst, compared to the TiO_2 nanoparticles, under UV illumination. On the other hand, the H_2RGOTi composite has shown the highest electrocatalytic activity towards oxygen reduction reaction in presence of UV illumination.

1. Introduction

The rapid expansion of industrialization and population growth produce a huge amount of wastewater. Phenol is one of the various refractory organic contaminants found in wastewater which requires special attention because of its toxic effects to humans and the environment [1-5]. The presence of phenol has been confirmed in many different industrial wastewaters e.g. chemical and petrochemical industries. The traditional water treatment techniques, including activated adsorption, chemical oxidation and biological digestion, have not been successful to meet the World Health Organization (WHO) standards [3, 6, 7]. Therefore, new treatment approaches for phenolic compounds in wastewater based on advanced oxidation processes (AOPs) were developed which can achieve higher efficiencies than the currently used ones. An example of AOPs in wastewater treatment is the use of a combination of hydrogen peroxide and ultraviolet radiation in the presence of TiO_2. This system has proven to be efficient in wastewater treatment [8, 9]. Unlike chlorine, which is widely used worldwide, hydrogen peroxide is an eco-oxidant that does not generate carcinogenic residues and plays an important role in green chemistry.

Graphene and reduced graphene oxide have attracted attention due to the excellent electrical, mechanical, thermal and optical properties that can be transformed into potential energy and environmental applications e.g. electronics, super capacitors, sensors, solar cells, wastewater treatment and gas storage [10, 11]. In addition, it has been shown that reduced graphene oxide can amend the photocatalytic and electrocatalytic properties of several semiconductors e.g. ZnO, WO_3 and TiO_2 when it forms composites with them [12 - 22]; however, the effect of the different types of graphene oxide's reduction methods on their catalytic properties has never been studied previously. So, the main objective of this work is (i) investigating how the reduction methods of graphene oxide affect the photocatalytic and electrocatalytic behaviours of reduced graphene oxide/TiO_2 composites. The reason for the probable reduction method – dependent catalytic behaviour cannot be attributed only to the change in the band gap energy of the different composites but also due to the difference in the amount and types of the oxygen functional groups on the reduced GO surface and the changes in the surface areas as the reduction methods for graphene oxide differ. Furthermore, the different stabilities of some oxidants or their radicals e.g. H_2O_2 or $HO^{\bullet}$ on the surfaces of some semiconductors/graphene oxide composites compared to others can be an additional sound reason for the differences in their catalytic properties. To investigate this point, four different composites of TiO_2/ graphene oxide or its reduced form were prepared and their photocatalytic and electrocatalytic behaviours were studied: graphene oxide/TiO_2 (GOTi), hydrazine hydrate-reduced graphene oxide/TiO_2

[a] Department of Health Environment, College of Health Sciences, PAAET, P.O. Box 1428, Faiha 72853, Kuwait.
[b] Center for Advanced Materials, Qatar University, Doha, P.O. Box 2713, Qatar.
[c] Chemistry Department, Kuwait University, P.O. Box 5969 Safat, 13060, Kuwait
† Corresponding author: abubakr_2@yahoo.com, bakr@qu.edu.qa Tel: +974-44035672.

(HHRGOTi), hydrogen-reduced graphene oxide/TiO_2 (H_2RGOTi) and thermally reduced graphene oxide/TiO_2 (RGOTi).

Other objectives for this work can be summarized as follows: (ii) chemical characterization of the as-prepared composites using bulk and surface analytical methods, (iii) electrochemical characterization of the same composites towards the oxygen reduction reaction (ORR) in an acidic medium (to target the 2-electron oxygen reduction mechanism which produces H_2O_2 that is needed for the AOPs) and (iv) photochemical characterization for these composites towards the phenol oxidation in the presence and absence of H_2O_2 under UV illumination.

2. Experimental

2.1. Synthesis

Graphene oxide powder (GO) was prepared using a modified Hummers' method [23]. First, 2 g of graphite powder (200 mesh, 99.9999%, Alfa Aesar A Johnson Matthy Company), 1 g of sodium nitrate (99.995%, Sigma-Aldrich) and 50 mL of concentrated sulphuric acid (98%, BDH) were mixed and vigorously stirred at 0 °C for 30 min using an ice water bath. Then, 6 g of potassium permanganate crystals (99.0%, Sigma-Aldrich) were added slowly to the solution while stirring. The ice water bath was then removed, and the mixture was stirred at 35 °C for 30 min. When the mixture became a pasty dark green colour with the evolution of gas bubbles, a 100 mL of distilled water was added slowly, and the temperature of the mixture was kept below 100 °C for 15 min. The diluted mixture acquired, at this stage, a brown colour. After this, the mixture was treated with a 100 mL of hydrogen peroxide (30%, Sigma-Aldrich) and stirred until it turned out to be a bright yellow suspension. Finally, the suspension was filtrated and washed with an excess amount of warm distilled water and was dried overnight under vacuum at 60 °C.

Loading of GO on the TiO_2 support was carried out using an impregnation technique in which a suspension of dispersed GO and an appropriate amount of deionized water/absolute ethanol were sonicated for 1 h. Commercial TiO_2 nanoparticles (particle size: 21 nm, from Sigma Aldrich) were then added, and the suspension was stirred for 12 h at 280 rpm using a rotary evaporator. Finally, the solvents were evaporated by heating under vacuum at 60 °C, and then the dried powder was crushed.

The HHRGOTi composite was prepared by reducing graphene oxide (GO) using hydrazine hydrate (HH) and then loading it on the TiO_2 according to the following recipe; an appropriate amount of GO suspension was added to a mixture of 20 mL of deionized water and 50 µL of hydrazine hydrate (25%, Sigma-Aldrich) until a yellowish brown suspension was formed. Then, it was heated in a 1000 W domestic microwave oven in two cycles (20 s on and 10 s off) for a total time of 60 s. Then, 10 mL of absolute ethanol and TiO_2 powder were added to the black suspension, and was stirred for 24 h at room temperature. Finally, the suspension was centrifuged at 6000 rpm for 25 min, washed with deionized water and then with ethanol and dried overnight under vacuum at 60 °C. To obtain only HHRGO without the TiO_2 support, the same procedure was followed except adding TiO_2 was excluded from the procedure.

The H_2RGOTi composite was prepared by reducing the TiO_2-supported GO (GOTi) in a quartz reactor using a flow of H_2 gas at a rate of 100 mL min^{-1} for 30 min and at a temperature of 450 °C. The sample was cooled at room temperature in the reactor and stored under vacuum. The same procedure was followed to obtain an unsupported H_2RGO powder except the starting material was unsupported GO.

TiO_2-supported thermally reduced GO (RGOTi) was prepared in a Teflon-lined stainless steel autoclave as follows: TiO_2 was added to a mixture of deionized water/absolute ethanol and sonicated for 30 min. Afterwards, the GO suspension was added under vigorous stirring, and the pH was adjusted to 3.5 using ammonium solution and nitric acid. The suspension was transferred to a Teflon-lined stainless steel autoclave that was operated at a 120 °C for 24 h. Finally, the suspension was centrifuged, washed with 1 M HCl and deionized water and dried at 80 °C for 24 h.

The loading percentage of the carbonaceous materials on the TiO_2 support was 0.1% for all photocatalytic experiments.

2.2. Characterization

IR spectra were measured for KBr – supported test samples (<1 wt.%) at room temperature over a frequency range of 4000-400 cm^{-1} at a 4.0 cm^{-1} resolution with a scanning rate of 2 mm s^{-1}, using a 6300 type A JASCO FT-IR spectrometer.

X-ray diffraction (XRD) patterns were obtained with a Bruker D8 diffractometer equipped with a Lynxeye detector using CuK_α radiation (λ= 15.406 x 10^{-2} nm). The diffractometer was operated at 40 kV and 40 mA. The data were collected between 10 and 80 ° with a scan step of 0.015 ° and a step time of 0.2 s. For phase identification purposes, the present investigation adopted the automatic JCPDS library search and match. The following computer software packages were used: Standard SERACH and DIFFRACT AT software (Australia).

Raman spectra were recorded on an InVia Raman microspectrometer working under macro conditions (f = 3 cm) with an excitation line of 532 nm. The samples were measured directly (without any pre-treatment), and the laser power was ~ 2 mW (in all cases). The spectra were obtained from an average spectrum of 5 different registration of the Raman spectrum of the same sample (parameters of each registration: spectral range was from 100 – 3500 cm^{-1}; number of accumulations was 3 and exposure time was 10 s).

UV-Vis diffuse reflectance spectra (DRS) were measured for the KBr - supported test samples (< 1 wt.%) at room

temperature in the range 200 - 800 nm at a resolution of 0.05 nm using a Cary 5000 UV-Vis-NIR (Agilent, Australia) with an integrating sphere accessory.

X-ray Photoelectron Spectroscopy (XPS) was conducted using a Thermo Scientific ESCALAB-250Xi spectrometer. The radiation source was a monochromatic AlK_{α} operating at a power of 300 W (15 kV, 20 mA). The vacuum in the analysis chamber was lower than $7x10^{-9}$ bar during all measurements. The in-situ reduction was carried out in a high-pressure gas cell housed in the preparation chamber. The binding energies were referenced to the C1s peak of the carbon contamination at 284.8 eV within an experimental error of ± 0.2 eV.

The surface areas were measured using an automatic ASAP 2010 Micromeritics sorpometer (USA) which is equipped with an outgassing platform and an online data acquisition and handling system. It was operated using various computer-run methods to analyse the adsorption data.

For the electrocatalytic measurements, 1 mg of the composite was dispersed in 1 mL of 1% Nafion (diluted from 5 wt% Nafion using isopropyl alcohol, both from Sigma-Aldrich) and then sonicated for 2 hours. 5 µL of the dispersion was casted on a glassy carbon electrode (GC) that was held upside down and was allowed to dry for 2 hours. The electrode was electrochemically characterized towards ORR in the presence and absence of UV radiation (300 watt) using the linear sweep voltammetry (LSV) technique at a scan rate of 50 mV s^{-1} in an oxygen-saturated 0.5 M H_2SO_4 solution. During the LSV measurements, the potential was swept from the more noble to the less noble direction. The counter and reference electrodes were a Pt wire and a Ag/AgCl electrode, respectively. For comparison, a deaerated 0.5 M H_2SO_4 solution (purged with Ar gas for 30 min) was used. During the measurements, Ar gas was flowed continuously above the solution to prevent the diffusion of O_2 to the deaerated solution.

2.3 Photocatalytic Reactions

Phenol solutions of 20, 40 and 60 mg L^{-1} were prepared in deionized water. In each test, 0.1 g of the prepared catalyst was added to 100 mL of each solution and mixed using a magnetic stirrer in the dark for 30 min until the adsorption equilibrium was reached. Then, the suspension was illuminated using a high pressure mercury lamp (300 W) emitting ultraviolet radiation with a maximum radiation peak of 365 nm. No pH adjustment of the phenol solution was performed. The distance between the solution and the radiation source was 4.5 cm. The time at which the ultraviolet lamp was turned on was considered "time zero" the beginning of the experiment. Samples were taken at 10 min intervals from the reaction vessel and filtered to remove the suspended composite particles using nylon filter paper of a pore size 0.4 µm. The concentration of the phenol was determined using the UV-vis spectrophotometer with a UV absorbance range of 190 to 400 nm, and the 269 nm absorbance corresponded to the maximum absorption of phenol.

3. Results and Discussion

3.1 Characterization

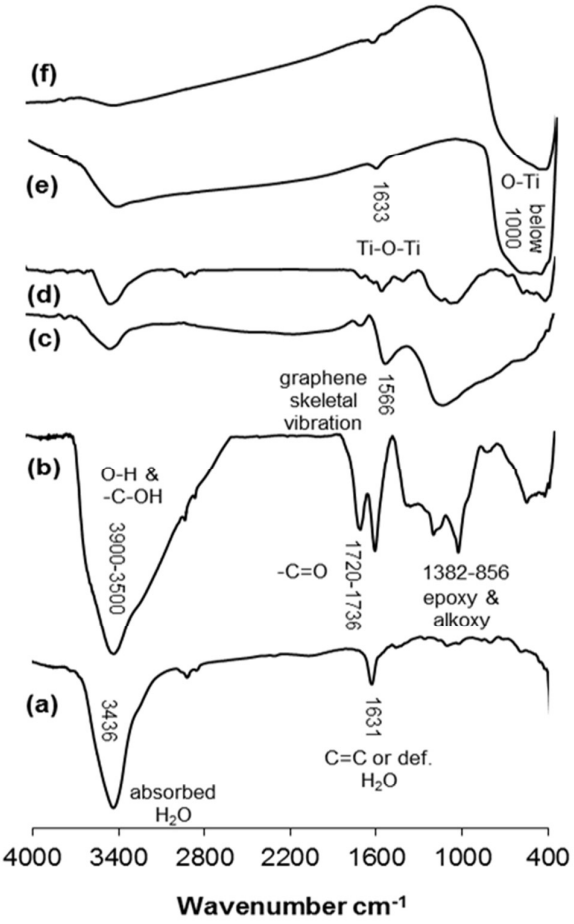

Figure 1. FT-IR spectra of (a) graphite, (b) GO, (c) H_2RGO, (d) HHRGO, (e) Ti, (f) GOTi.

Figure 1a shows the FT-IR spectrum of the initial graphite powder. A peak located at 3436 cm^{-1} corresponds to the absorbed water while the peak at 1631 cm^{-1} can be assigned either to the C=C stretching vibration band [24] or to the deformation of water molecules [25]. After the graphite powder oxidation process using the modified Hummers' method, the FT-IR spectrum of the produced GO powder was measured as shown in Figure 1b. A red shift in the C=C peak was observed in which the peak was shifted from 1631 to 1621 cm^{-1}. The absorption band between 1720 and 1736 cm^{-1} corresponds to the carboxylic and carbonyl groups [26 - 28]. Additionally, the absorption peaks at 1382 – 856 cm^{-1} are ascribed to epoxy and alkoxy groups [29 – 33]. A broad band between 3900 – 3500 cm^{-1} is due to the O-H stretching vibrations of C-OH groups (from hydroxyl and/or carboxylic groups) and intercalated water molecules [24, 32, 34]. These results confirm that the oxidation of

graphite powder took place and the functional groups on the GO surface are mainly composed of hydroxyl, epoxy, carbonyl and carboxylic groups [35]. However, the graphite oxidation process is incomplete, and this was confirmed by the peak at 1621 cm^{-1}, which corresponds to the remaining sp^2 character [36]. After reducing the GO either by hydrogen gas (Fig. 1c) or hydrazine hydrate (Fig. 1d), the number of the oxygen functional groups decreased drastically [37] and a new absorption peak at approximately 1566 cm^{-1} was detected that may be attributed to the skeletal vibration of the graphene sheets [13, 36, 38 – 40]. Figures 1e and 1f compare the FT-IR spectra of TiO_2 and TiO_2-supported GO (GOTi), respectively, in which a strong broad absorption band at low frequency (below 1000 cm^{-1}) was measured. This band was attributed to the vibration of Ti-O-Ti in TiO_2, similar to that of pure commercial P25-TiO_2 [18, 29, 39, 41]. The absorption band at 1633 cm^{-1} can be attributed to the Ti-O-Ti stretching vibration [25] or to the deformation of water molecules. No absorption peak corresponding to the GO was observed. This is most likely due to the low amount of GO in the composite materials (0.1%).

reduction of GO with hydrogen (Fig. 2c), the diffraction peaks at 2θ = 11.6 and 26.6 ° disappeared and a new broad peak at 2θ = 25.8 ° with a corresponding d-spacing of 3.53 Å was recorded. This peak was also observed by Thema et al. upon reduction of GO using hydrazine hydrate [37]. The XRD pattern of HHRGO (Figure 2d) also showed the disappearance of the diffraction peaks at 26.6 and 11.6 ° and the presence of a new small broad peak at 2θ = 13.0 ° with a d-spacing of 6.80 Å. From these observations, we can conclude that the structure of HHRGO is different from H_2RGO, and the reduction process was not complete in both cases because the d-spacing is higher than that of the parent graphite powder. In addition, based on the d-spacing, the extent of reduction for H_2RGO is higher than HHRGO. Most likely, in the case of HHRGO, the small peak at 2θ = 13.0 ° is due to the formation of a new structure of GO with a lower oxygen content because its corresponding d-spacing (6.80 Å) lies within the range of 6.3 to 9.0 Å for GO [28, 38, 43] that is prepared from graphite using the Hummers' method [23]. Additionally, HHRGO has an amorphous structure that is consistent with other reports in the literature [42, 44, 45].

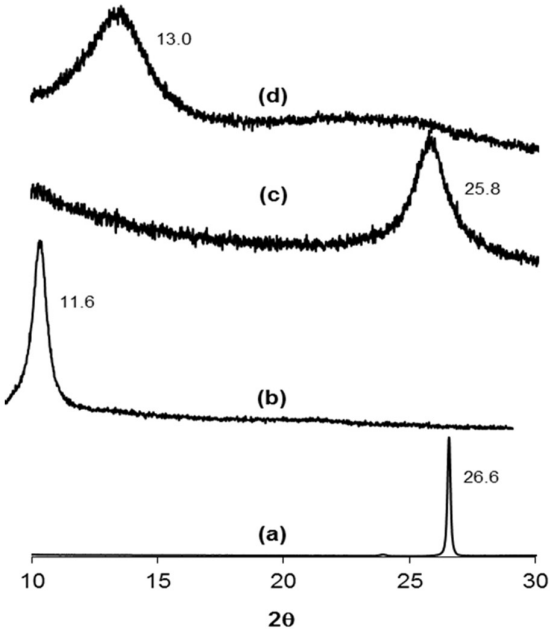

Figure 2. XRD patterns of (a) graphite, (b) GO, (c) H_2RGO, (d) HHRGO

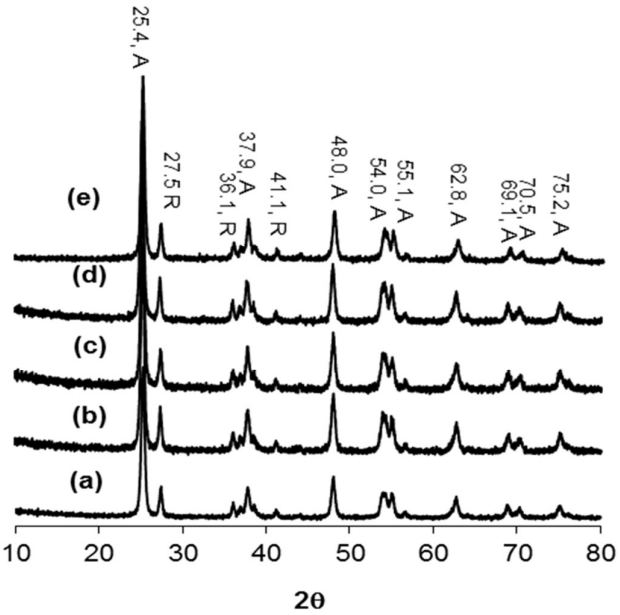

Figure 3. XRD patterns of (a) TiO_2, (b) GOTi, (c) H_2RGOTi, (d) HHRGOTi, (e) RGOTi

Figure 2 displays the XRD patterns of the unsupported (a) graphite, (b) as-prepared GO, (c) H_2RGO, and (d) HHRGO. The graphite powder in Figure 2a shows a typical diffraction peak at 2θ = 26.6 ° with an interlayer spacing of 3.35 Å that corresponds to the 002 facet. This peak disappeared upon oxidation, and a new peak at 2θ = 11.6 ° corresponds to the interlayer spacing of 7.78 Å was appeared as shown in Figure 2b. The increase in the d-spacing is due to the presence of oxygen functional groups that facilitated the hydration and exfoliation of the graphene sheet in aqueous media and confirms the oxidation of the graphite powder [30, 42]. After

Figure 3 shows the XRD patterns of (a) TiO_2, (b) GOTi, (c), H_2RGOTi, (d) HHRGOTi, and (e) RGOTi. The XRD patterns of all composites look similar to that of the neat TiO_2 (Fig. 3a), which consists of a mixture of anatase (A) and rutile (R) phase with no detected diffraction pattern for the carbon material. Similar results were observed in previous reports [13, 15, 19, 25, 41, 46]. Therefore, we conclude that the addition of carbon species did not change the crystalline phases of TiO_2, and the disappearance of their diffraction patterns may be attributed to: 1) their low percentage in the composite materials (0.1%), 2) their low diffraction intensity (below the detection limit of

the instruments) or 3) their overlapping patterns with the anatase phase pattern at 2θ value of 25.4 ° [13, 16-19, 47, 48].

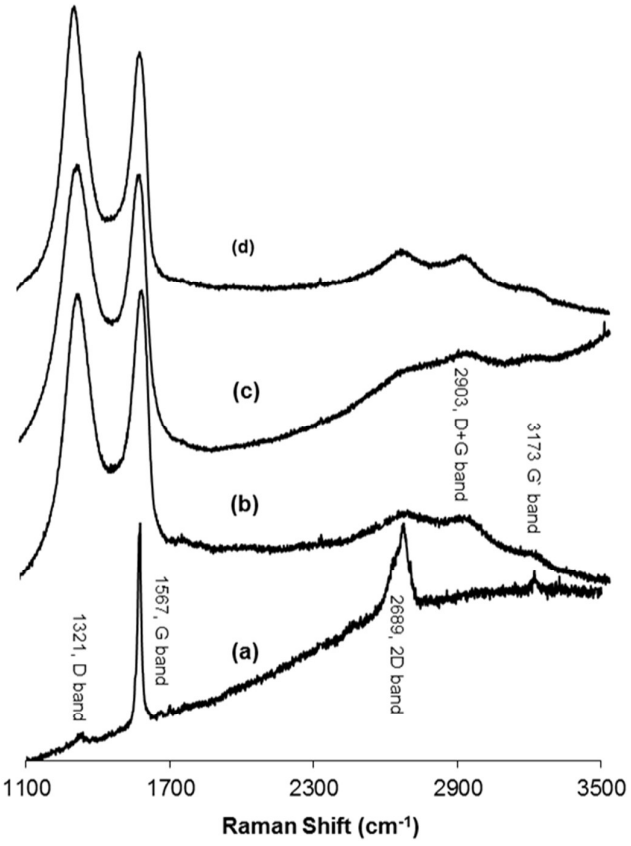

Figure 4. Raman spectra at 532 nm of (a) graphite, (b) GO, (c) H_2RGO450, (d) HHRGO

Raman spectroscopy was used to distinguish between the ordered and disordered crystal structures of carbon. Spectra that were measured at 532 nm contained the D band, which is a disordered mode that is related to the presence of sp^3 defects. This results from a breathing mode of κ-point phonons of A1g symmetry. The G band is assigned to the E2g phonon of C sp^2 atoms, while the 2D band corresponds to the overtone of the D band and appears in the second-order Raman spectra of the crystalline graphite (free of disorder) [33, 49-52]. Furthermore, the ratio of the intensities of the D and G ban (ID/IG) can be used as an indication of the amount of functionalization in a carbon material. A high ID/IG ratio means a high degree of disorder, i.e., a high degree of functionalization [53, 54]. Figure 4 shows the Raman spectra of (a) graphite, (b) GO, (c) H_2RGO, and (d) HHRGO. As shown in Figure 4a, the spectrum of the graphite exhibited a strong G band at 1567 cm^{-1}, a very weak D band at 1321 cm^{-1} and a 2D band at 2689 cm^{-1}. Upon graphite oxidation (Fig. 4b), the D and G bands widened and shifted towards higher wave numbers at 1339 cm^{-1} and 1588 cm^{-1}, respectively. The blue shift in the G band is attributed to the existence of isolated double bonds that resonate at higher frequency than the G band in graphite [55, 56]. The decrease in the G band intensity and the increase of the D band confirms a reduction in the size of the in-plane sp2 domains due to the incorporation of functional groups that form sp3 bonds in the carbon network [33, 57]. In addition, broad peaks at approximately 2903 and 3173 cm^{-1} were detected that correspond to a D + G combination mode that is induced by a disorder [50] and an overtone of the G line (G`), respectively.

When GO was reduced by hydrogen (Fig. 4c), the D band location did not change while the G band was shifted to a lower frequency region (1579 cm^{-1}), confirming the reduction process [47, 58]. A decrease in the relative intensity of the D band was observed, which resulted in a decrease in the D/G intensity ratio of H_2RGO (0.87) compared to the GO (0.90). These changes suggest an increase in the sp^2 domain (i.e., more graphitization due to the reduction process), and the results prove that the structure of H_2RGO is more ordered with less defects than the structure of GO [53]. However, for HHRGO (Fig. 4d), the D and G bands shifted slightly to a lower frequency and the ratio of the D/G bands (1.04) was increased compared to the GO (0.90). These changes are attributed to the decrease in the average size of the sp^2 domain where new graphitic domains were created that are higher in number and smaller in size than those present in GO [33, 51, 59]. Therefore, we conclude that the structures of H_2RGO and HHRGO are different, and the structure of the H_2RGO is more ordered than the HHRGO. This was further supported by the results obtained from the XRD (compare Figures 2c and 2d). According to Pimenta et al. [50], the crystalline size can be determined by Equation 1:

$$L_a\ (nm) = (2.4 \times 10^{-10})\lambda_{laser}^4 \left(\frac{I_D}{I_G}\right)^{-1} \quad [1]$$

where La is the size of the crystalline domains, λ is the excitation wavelength (532 nm), and I is the intensity ratio of D and G bands in the Raman spectrum. From the D/G intensity ratio determined from the Raman spectra, the crystalline domains were calculated and found to be 22 and 18 nm for the H_2GRO and HHRGO, respectively. Furthermore, the position and the shape of the 2D peak can be used to distinguish the number of layers of the reduced graphene oxide. The broader 2D peak located at 2683 cm^{-1} for both H_2RGO and HHRGO indicated that the samples are likely between 2 and 5 layers thick [51]. Figure 5 shows the Raman spectra of (a) TiO_2, (b) GOTi, (c) H_2RGOTi, and (d) HHRGOTi. Figure 5a reveals several characteristic bands at 144, 198, 394, and 639 nm which are attributed to anatase and 144, 443 and 610 nm that are attributed to the rutile [25, 60]. Unlike XRD, loading of the carbon species on the TiO_2 produced their characteristic vibration bands in the Raman spectra (Fig. 5). The GOTi showed D and G bands at 1345 and 1599 cm^{-1}, respectively. The same bands were observed for both H_2RGOTi and HHRGO.

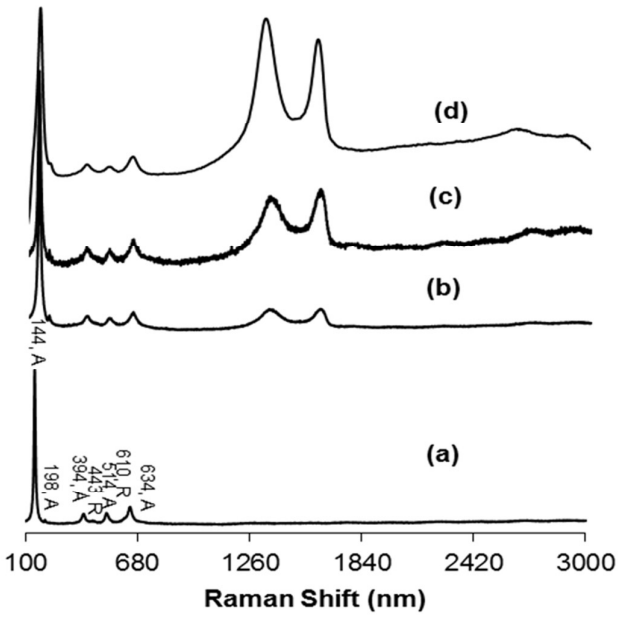

Figure 5. Raman spectra at 532 nm of (a) Ti, (b) GOTi, (c) H_2RGOTi, (d) HHRGOTi

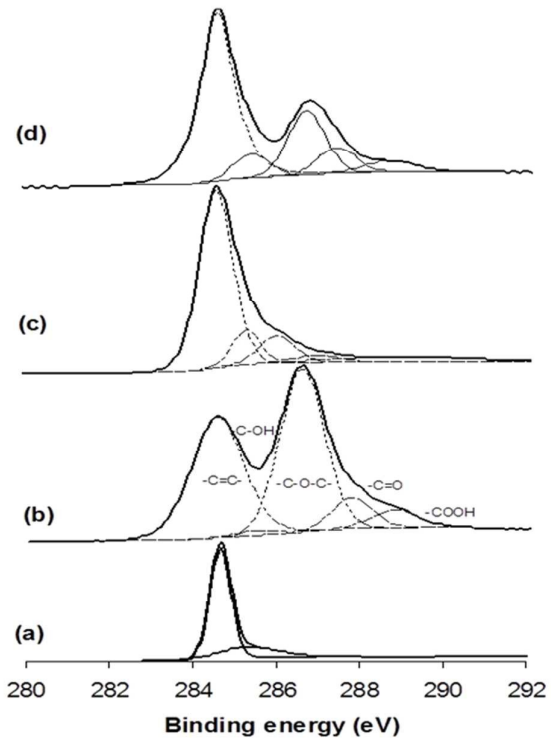

Figure 6. Carbon region of XPS spectra of (a) graphite, (b) GO, (c) H_2RGO, (d) HHRGO

Figure 6 reveals the C region of the XPS spectra of graphite, GO, H_2RGO and HHRGO. Graphite exhibited a strong spectral line at 284.68 eV for carbon and a small broad peak at 258.33 eV for some adsorbed species on the sample's surface that likely represent water molecules (Fig. 6a). In the GO spectrum (Fig. 6b), the peak with a binding energy of 284.64 eV can be attributed to the C-C and C=C bonds, while peaks centered at binding energies of 285.49, 288.60, 287.52 and 288.69 eV can be assigned to the -C-OH, -C-O-C-, -C-C=O and -COOH, respectively [61]. This proves the successfulness of the oxidation process of graphite. During the in-situ reduction using hydrogen at 450 ^{o}C for 30 min, carboxylic, carbonyl and epoxy groups were reduced while hydroxyl groups were increased (Fig. 6c). This clearly confirms a considerable degree of reduction of GO, but the reduction process was incomplete when small amounts of oxygen functional groups were still detected. The same situation was observed during the reduction of GO with hydrazine hydrate (Fig. 6d), but the extent of reduction when hydrogen gas was used was more than when hydrazine hydrate was used. These results are consistent with the results obtained from the XRD and the Raman spectra.

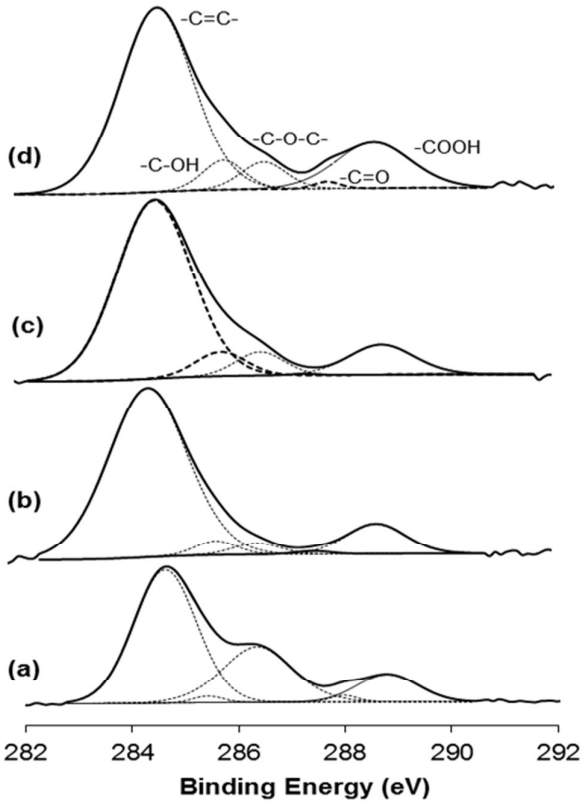

Figure 7. Carbon region of XPS of (a) GOTi, (b) H_2RGOTi, (c), HHRGOTi, (d) RGOTi.

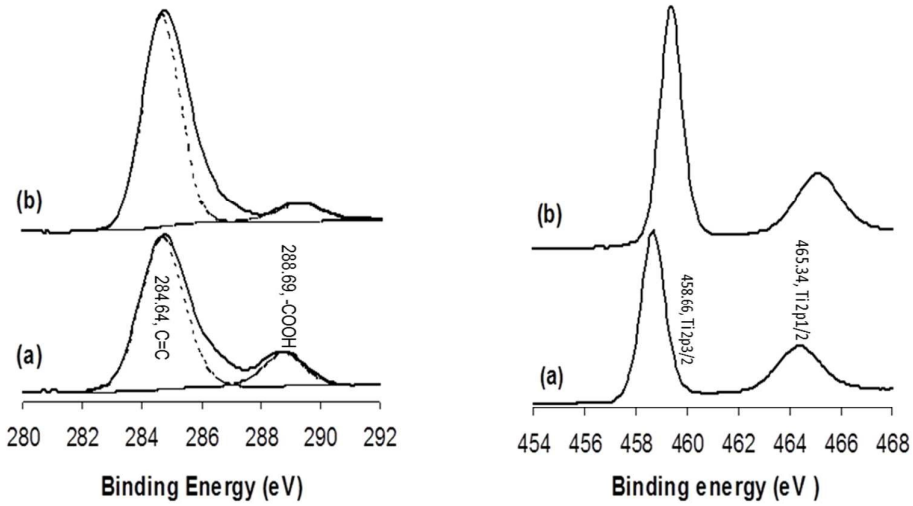

Figure 8. XPS of the Carbon (on left) and Ti regions (on right) for commercial TiO_2 (a) before and (b) after hydrogen reduction using a stream of H_2 gas at 450 °C for 1 h.

Figure 7 shows the XPS spectra of (a) GOTi, (b) H_2RGOTi, (c) HHRGOTi and (d) RGOTi. In Figure 7a, the same functional groups are shown as for unsupported GO (shown in Figure 6b). However, after reduction (Fig. 7b), the peak corresponding to a carboxylic acid group did not disappear. In fact, its intensity was increased compared to the corresponding spectra shown for the reduced GOTi. This is opposite to what was observed for unsupported RGO (Fig. 6c). To explain this observation, the XPS of commercial TiO_2 was measured and subjected to a hydrogen flow at 450 °C for 1 h (Figure 8). It is obvious from the carbon region in the XPS spectra of TiO_2 that the carboxylic acid groups exist in commercial TiO_2, and they were not reduced after their exposure to the stream of H_2 gas at 450 °C for 1 h (Figure 8a). A small shift of 0.75 eV for the Ti 2p 3/2 (458.66 eV) and Ti 2p 1/2 (465.34 eV) spin orbit coupling peaks to higher binding energies after exposure to hydrogen gas at 450 °C was observed (Figure 8b). However, the spacing between them remains the same before and after reduction with hydrogen (5.68 eV). Therefore, we conclude that the carboxylic acid groups are strongly bonded to the TiO_2 most likely through the oxygen of the TiO_2. As expected, the oxidation number of titanium did not change because the reduction of Ti (IV) to lower valence state(s), such as Ti_2O_3, does not commence at temperatures less than 1000 ^oC [62]. Furthermore, the reduction process can even promote the bonding between TiO_2 and carboxylic acid groups because it has been observed that the amount of carboxylic groups is increased after reduction compared to GOTi.

An etching experiment using argon bombardment was carried out for GOTi to obtain information regarding which material is the top layer. It is clear from Table 1 that GO is on the surface of TiO_2 because the amount of Ti increased while the amount of GO decreased as the etching time increases.

Table 1. Etching of GOTi at different times by Ar bombardment.

Titanium (%)	Etching Time (s)	Etching Depth (nm)	Carbon (%)
43.19	15	1	4.71
47.60	40	3	0.90
48.34	65	5	0.68
49.51	90	7	0.34
50.09	125	10	0.31
50.36	230	20	0.23

Table 2. Surface areas of materials used.

Material	BET ($m^2 g^{-1}$)
graphite	20.5
GO	40.3
H_2RGO	343.0
HHRGO	256.4
TiO_2	51.1
GOTi	50.0
RGOTi	50.2
H_2RGOTi	47.7
HHRGOTi	50.9
RGO	49.1

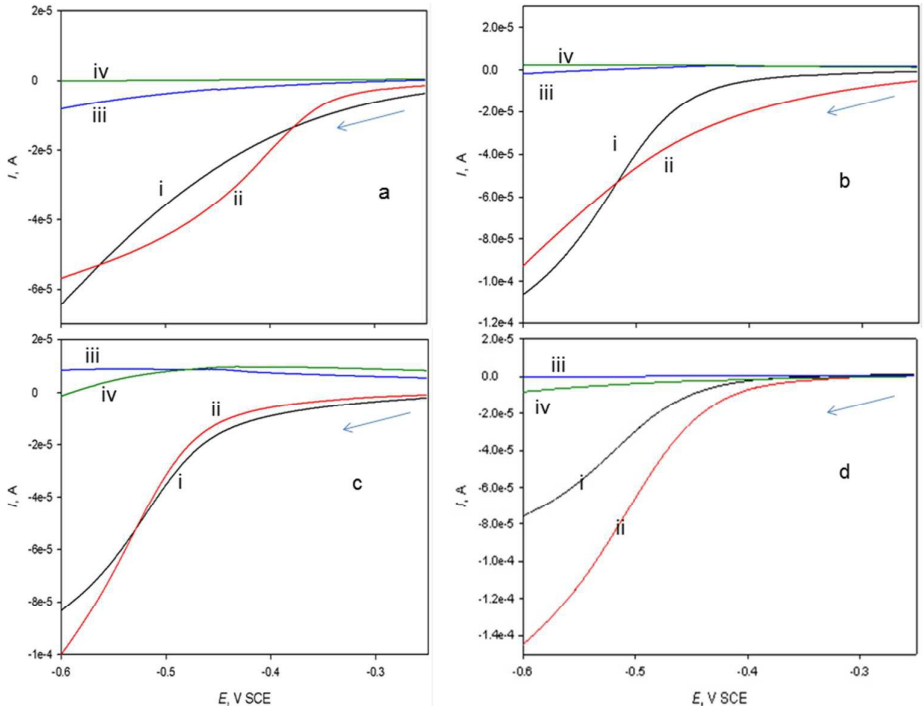

Figure 9. Linear Sweep Voltammograms (LSVs) at a scan rate of 50 mV s-1 for (a) GC, (b) Ti/GC, (c) GOTi/GC and (d) H_2RGOTi/GC electrodes in (i & ii) oxygen and (iii & iv) argon-saturated 0.5 M H_2SO_4 at 25 °C in the presence (ii & iv) and absence (i & iii) of 300 Watt UV radiation.

The surface areas of the different prepared and used materials in this study are summarized in Table 2. It was observed that surface area of graphite is increased from 20.5 to 40.3 m^2 g^{-1} upon its oxidation, and it is further increased when the GO is reduced by hydrazine hydrate or hydrogen gas. However, the surface area of H_2RGO is 343 m^2 g^{-1}, which is more than that of HHRGO (256.4 m^2 g^{-1}). There were no significant changes in the BET surface areas of the TiO_2, GOTi and the reduced GOTi composites. Similar observations have been noted by other researchers [18, 26].

Figure 9 displays the linear sweep voltammograms for (a) GC, (b) TiO_2/GC (Ti) (c) GOTi/GC and (d) H_2RGOTi/GC electrodes in (i & ii) oxygen and (iii & iv) argon-saturated 0.5 M H_2SO_4 at 25 °C in presence (ii & iv) and in absence (i & iii) of 300 Watt UV radiation. The potential sweep started from the more noble direction where a very small current flows to the less noble direction where the over potential increases and the oxygen reduction reaction is expected to start. This assisted in the determination of the ORR onset potential accurately. The UV-radiation affects the oxygen reduction reaction significantly as seen from the difference between the black and the red *E-I* curves in Figure 9. Generally, it is reported that the mechanism of ORR on TiO_2 surface under UV radiation follows a series of single electron steps as follows: (e: electron, h: hole, cb: conduction band and vb: valence band) [63]:

$$TiO_2 + h\upsilon \rightarrow e^-_{cb} + h^+_{vb} \quad [2]$$

$$O_2 + e^-_{cb} \rightarrow O_2\bullet^- \quad [3]$$

$$H^+ + O_2\bullet \rightarrow HO_2\bullet \text{ (at pH < 4.8)} \quad [4]$$

$$2HO_2\bullet \rightarrow H_2O_2 + O_2 \quad [5]$$

$$HO_2\bullet + e^-_{cb} + H^+ \rightarrow H_2O_2 \quad [6]$$

The best onset reduction potential (the most noble) for ORR is for GC (-350 mV), but the highest current at any given potential was observed for H_2RGO/Ti (e.g., -1.4x10^{-4} A at a potential of -0.6 V). Furthermore, only H_2RGOTi exhibited a high ORR rate under UV illumination at any potential. This was attributed to the lowering in the band gap energy of TiO_2 when composited with reduced graphene oxide. Table 3 shows the

band gap energies for the different catalysts and composites that were used in this work.

Table 3. Wavelengths at the absorption edge for the Ti, GOTi, RGOTi, HHRGOTi and H_2RGOTi and the corresponding band gap energies.

Catalysts	Wavelength (nm)	Band Gap Energy
Ti	393	3.16
GOTi	403	3.08
RGOTi	391	3.11
HHRGOTi	414	3.0
H_2RGOTi	410	3.03

The UV radiation boosted the ORR kinetics for Ti (P25-TiO_2) at less noble potentials but decreased it at the more noble potentials (Figure 9b). On the contrary, the results were reversed for GOTi/GC in which the kinetics of the ORR was enhanced as the potential was scanned in the less noble direction. For the GC, both behaviors were observed in which the UV radiation only enhanced the ORR kinetics between -0.390 and -0.565 V. At potentials more noble than -0.390 V and less noble than -0.565, the ORR kinetics were retarded in the presence of UV radiation compared to when UV radiation was absent. Furthermore, the GOTi (Figure 9c) did not show any significant difference between the ORR kinetics in the presence or absence of UV radiation at small overpotential. However, the noticed enhancement in the ORR kinetics at high overpotentials is attributed to the reduction of GO in the GOTi composite, i.e., the composite changed from GOTi to RGOTi (similar to Figure 9d plot ii). This can be confirmed by comparing plots ii and iv in Figure 9c where in absence of O_2 (plot iv of Figure 9c), the current started to increase at a potential of -0.53 V. This is almost the same potential at which the current in the presence of UV started to be higher than the corresponding potential in the absence of UV. Figure 9 does not show the results for HHRGOTi/GC or RGOTi/GC because those electrocatalytic results were not comparable with those of GC and the H_2RGOTi electrodes. This indicated that the reduction method of graphene oxide affected significantly the electrocatalytic behavior of the composite. It is worthy to mention that the measurements were repeated with the UV lamps of different powers, and the resulting trends did not change.

3.2 Photocatalytic Reactions

In all cases, a 0.1 % loading of carbonaceous species was used in the composite. Higher loading percentages of the "black" carbonaceous material increased its light absorption and consequently decreased the photocatalytic activity of TiO_2. No detectable degradation of phenol was observed in the absence of TiO_2 in any of the as-prepared composites. The kinetic plots corresponding to the degradation of a 20 mg L^{-1} of phenol (in water) in presence of (i) commercial TiO_2 nanoparticles, (ii) GOTi, (iii) HHRGOTi, (iv) H_2RGOTi or (v) RGOTi photocatalysts and in absence of H_2O_2 are plotted against UV irradiation time in Figure 10.

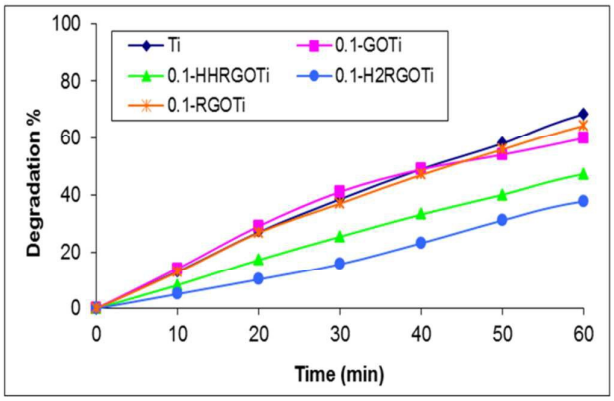

Figure 10. Kinetics of phenol degradation (20 mgL^{-1}) under 300 W UV illumination in the presence of (a) Ti, (b) GOTi, (c) H_2RGOTi, (d) HHRGOTi and (e) RGOTi catalysts.

The degradation % represents (C_0 - C_t/C_0) * 100, where C_0 is the remaining concentration of phenol after adsorption equilibrium before UV illumination. The C_t represents the remaining phenol concentration after UV illumination for a specific time. We observed that the phenol degradation is increased with UV irradiation time for all catalysts. The best phenol degradation percentage (fastest rate) was obtained in the case of TiO_2, then RGOTi catalysts and the lowest degradation rate was observed for the H_2RGOTi catalyst. However, the difference in the performance between TiO_2 and RGOTi is small under the experimental conditions studied. A 38.5 % conversion of phenol was observed after 30 min of UV illumination in the presence of commercial TiO_2 and was

increased to 58.1 % after 50 min. For RGOTi, 37.0 % of phenol degradation was achieved after 30 min of UV irradiation and was increased to 56.0 % after 50 min. Different results were obtained with the addition of 70 µL H_2O_2 (Fig. 11). A faster phenol degradation was attained using RGOTi (Fig. 11e) than using the commercial TiO_2 (Fig. 11a) at all times. For example, 42.6 % and 71.1 % conversions were obtained after 30 min and 50 min UV illumination respectively in the presence of RGO with addition of H_2O_2 compared to 31.8 % and 66.0 % conversions in case of TiO_2 under same experimental conditions. Furthermore, In case of RGO at 30 and 60 min, phenol degradation rate is higher by 15 % and 27 %, respectively, compared to the experiment in which H_2O_2 was not added (Fig. 10).

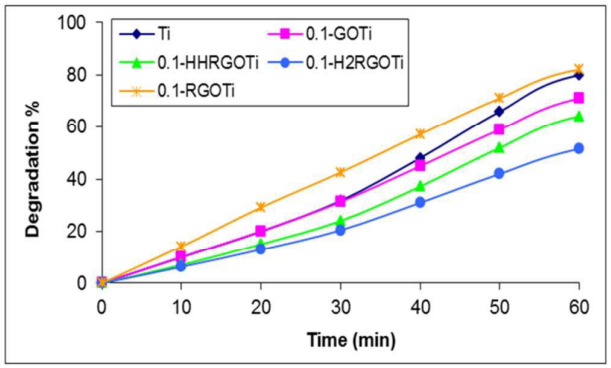

Figure 11. Kinetics of phenol degradation (20 mg L^{-1}) under 300 W UV illumination in the presence of (a) Ti, (b) GOTi, (c) H_2RGOTi, (d) HHRGOTi and (e) RGOTi catalysts. A 70 µL of H_2O_2 was used with all catalysts.

Upon addition of 70 µL of the H_2O_2 ¬and keeping constant all other experimental conditions, comparative studies were carried out between TiO_2 and RGOTi with different phenol concentrations (See Figures S1 and S2 in the supporting information). For both TiO_2 and RGOTi, phenol degradation rate decreased with increasing the phenol concentration. However, for 40 mg L^{-1} phenol, the decrease in the degradation rate was more obvious for the commercial TiO_2 than for the RGOTi. For example, after 60 min UV illumination a 39.2 % conversion was attained in case of TiO_2 while a 52.5 % conversion was obtained in the case of RGOTi. It is worthy to mention here that, although H_2RGOTi and HHRGOTi have the lowest band gap energies and consequently were expected to have the best catalytic behavior compared to TiO_2, the opposite exactly happened where they have shown the worst photocatalytic performance. This confirms that the band gap energy is not the only controlling factor when comparing between the different photocatalysts shown here. Furthermore, the surface area of the catalysts (see Table 3) is the controlling factor when H_2O_2 is absent but in presence of it, RGOTi had the highest photocatalytic activity. The reason for this is attributed to the more stability of H_2O_2 in presence of RGOTi compared to TiO_2.

The effect of H_2O_2 concentration on the rate of phenol degradation was studied (See Figure S3 in the supporting information). A little higher degradation rate was observed upon adding 100 µL H_2O_2. The addition of 70 µL and 40 µL of H_2O_2 had nearly the same effect on the rate of phenol degradation before 40 min. At time higher than 40 min, phenol degradation rate was decreased in case of using 40 µL of H_2O_2.

It is worth mentioning that the kinetics curves in case of the bare TiO_2 and the different composites, except RGOTi, (Figure 11) have two slopes: one at the beginning of the experiment up to 30 minutes and another one after 30 min. The slope after 30 min. is higher than the one before where a kind of activation for the catalyst has taken place after 30 min. In case of RGOTi, the kinetics curves are always linear (i.e. one slope) as can be seen in Figures 11, S2 and S3.

The effect of the UV radiation power was also studied using 0.1 g of RGOTi in the presence of 70 µL H_2O_2. Changing the UV lamp power from 150 to 300 to 500 W did not change the rate of phenol degradation on the RGOTi catalyst (See Figure S4 in the supplemental information).

4. Conclusions

Four composites with different band gap energies were prepared using (a) commercial TiO_2 and (b) one of the following synthesized carbonaceous materials: GO, H_2RGO, HHRGO or RGO. The hydrogen reduction method resulted in a more ordered graphene structure that has a higher surface area compared with the thermally and chemically reduced GO. Chemical and physical characterization techniques documented many differences between GO that were reduced using different reduction methods.

In terms of the measured oxygen reduction currents, H_2RGOTi composite has shown a superior electrocatalytic behaviour towards ORR under UV illumination compared with GC and the other reduced graphene oxide/TiO_2 composites. At -0.6 V SCE, the highest rate for ORR followed this order: H_2RGOTi/GC > GOTi/GC ≈ Ti/GC > GC which might be useful for the in-situ generation of H_2O_2 during an advanced oxidation process.

Also, the effect of the GO reduction method on the photocatalytic activity of the aforementioned composites towards the degradation of phenol in the presence and absence of (i) UV and (ii) H_2O_2 was examined. Although the band gap energy for HHRGOTi and H_2RGOTi are the lowest (3 and 3.03 eV) compared to TiO_2 (3.16 eV), high phenol degradation rates were achieved using TiO_2 the RGOTi photocatalyst (3.11 eV) under UV illumination in absence and presence of H_2O_2, respectivel. This proved that the band gap energy is not the only controlling parameter for the photocatalysts used for phenol degradation. In fact the reason that RGOTi has the best photocatalytic behavior in presence of H_2O_2 can be attributed to the number and type of oxygen functional groups on the surface of RGOTi in addition to the stability of H_2O_2 or its radicals on the surfaces of RGOTi compared to TiO_2 and the other prepared photocatalysts.

5. Acknowledgments

This work was supported and co-funded by the Kuwait Foundation for Advancement of Sciences (KFAS) through project No. 2012-1405-01 and the Public Authority of Applied Education and Training (PAAET) through research project No. HS-12-02. Research Title: Photocatalytic Oxidative Removal of Phenolic Compounds from Wastewater Using Ozone and Hydrogen Peroxide Produced by Advanced Electrodes.

6. References

1. Z. Wu, Y. Cong, M. Zhou, Q. Ye and T. Tan, Korean J. Chem. Eng., 2002, 19, 866-870.

2. A. Ortiz-Gomez, B. Serrano-Rosales, M. Salaices and H. de Lasa, Ind. Eng. Chem. Res., 2007, 46, 7394-7409.

3. M. Tian, G. Wu, B. Adams, J. Wen and A. Chen, J. Phys. Chem. C, 2008, 112, 825-831.

4. J. Yang, J. Dai, C. Chen and J. Zhao, J. Photochem. Photobiol., A, 2009, 208, 66-77.

5. M. Pera-Titus, V. García-Molina, M. A. Baños, J. Giménez and S. Esplugas, Appl. Catal., B, 2004, 47, 219-256.

6. J. Yan, W. Jianping, B. Jing, W. Daoquan and H. Zongding, Biochemical Engineering Journal, 2006, 29, 227-234.

7. W. Z. Tang and A. Huren, Chemosphere, 1995, 31, 4171-4183.

8. L. Jack H, J. Catal., 2003, 216, 455-460.

9. M. A. O. Badmus, T. O. K. Audu and B. U. Anyata, Afr. J.Biotechnol., 2007, 6, 238-242.

10. A. Wei, J. Wang, Q. Long, X. Liu, X. Li, X. Dong and W. Huang, Mater. Res. Bull., 2011, 46, 2131-2134.

11. Z.-S. Wu, W. Ren, L. Gao, B. Liu, C. Jiang and H.-M. Cheng, Carbon, 2009, 47, 493-499.

12. V. Štengl, S. Bakardjieva, T. M. Grygar, J. Bludská and M. Kormunda, Chem. Cent. J., 2013, 7, 1-12.

13. S. Liu, H. Sun, S. Liu and S. Wang, Chem. Eng. J., 2013, 214, 298-303.

14. C. H. Kim, B.-H. Kim and K. S. Yang, Carbon, 2012, 50, 2472-2481.

15. H. Zhao, F. Su, X. Fan, H. Yu, D. Wu and X. Quan, Chinese J. Catal., 2012, 33, 777-782.

16. D. Wang, X. Li, J. Chen and X. Tao, Chem. Eng. J., 2012, 198–199, 547-554.

17. F. Wang and K. Zhang, J. Mol. Catal. A-Chem., 2011, 345, 101-107.

18. H. Zhang, X. Lv, Y. Li, Y. Wang and J. Li, ACS Nano, 2009, 4, 380-386.

19. N. R. Khalid, E. Ahmed, Z. Hong, L. Sana and M. Ahmed, Curr. Appl. Phys., 2013, 13, 659-663.

20. F. S. Omar, H. Nay Ming, S. M. Hafiz and L. H. Ngee, International J. Photoenergy, 2014, 2014, 8.

21. M. K. Kavitha, S. C. Pillai, P. Gopinath and H. John, J. Environ. Chem. Eng., 2015, 3, 1194-1199.

22. Y. H. Ng, A. Iwase, N. J. Bell, A. Kudo and R. Amal, Catal. Today, 2011, 164, 353-357.

23. W. S. Hummers and R. E. Offeman, J. Am. Chem. Soc., 1958, 80, 1339-1339.

24. N. Hu, Y. Wang, J. Chai, R. Gao, Z. Yang, E. S.-W. Kong and Y. Zhang, Sensor. Actuat. B-Chem., 2012, 163, 107-114.

25. H. Liu, X. Dong, X. Wang, C. Sun, J. Li and Z. Zhu, Chem. Eng. J., 2013, 230, 279-285.

26. H.-L. Ma, Y. Zhang, Q.-H. Hu, D. Yan, Z.-Z. Yu and M. Zhai, J. Mater. Chem., 2012, 22, 5914-5916.

27. M. Z. Kassaee, E. Motamedi and M. Majdi, Chem. Eng. J., 2011, 172, 540-549.

28. T. Kyotani, K.-y. Suzuki, H. Yamashita and A. Tomita, Tanso, 1993, 160, 255-265.

29. J. Guo, S. Zhu, Z. Chen, Y. Li, Z. Yu, Q. Liu, J. Li, C. Feng and D. Zhang, Ultrason. Sonochem., 2011, 18, 1082-1090.

30. V. Loryuenyong, K. Totepvimarn, P. Eimburanapravat, W. Boonchompoo and A. Buasri, Adv. Mater. Sci. Eng., 2013, 1-5.

31. J. Song, X. Wang and C.-T. Chang, J. Nanomater., 2014, 1-6.

32. Y.-p. Zhang, J.-j. Xu, Z.-h. Sun, C.-z. Li and C.-x. Pan, Prog. Nat. Sci. Mater. Inter., 2011, 21, 467-471.

33. J. Oh, N. D. Luong, T.Hwang, J.Hong and J. Nam, Jeju, South Korea, 2011.

34. M. El Achaby, F. Z. Arrakhiz, S. Vaudreuil, E. M. Essassi and A. Qaiss, Appl. Surf. Sci., 2012, 258, 7668-7677.

35. H. Al-Kandari, A. M. Abdullah, A. M. Mohammad and S. Al-Kandari, ECS Trans., 2014, 61, 13-26.

36. Y. Yao, S. Miao, S. Liu, L. P. Ma, H. Sun and S. Wang, Chem. Eng. J., 2012, 184, 326-332.

37. F. T. Thema, M. J. Moloto, E. D. Dikio, N. N. Nyangiwe, L. Kotsedi, M. Maaza and M. Khenfouch, J. Chem., 2013, 2-6.

38. C. Nethravathi and M. Rajamathi, Carbon, 2008, 46, 1994-1998.

39. K. Zhou, Y. Zhu, X. Yang, X. Jiang and C. Li, New J. Chem., 2011, 35, 353-359.

40. S. Reich and C. Thomsen, Phil. Trans. R. Soc. Lond. A, 2004, 362, 2271-2288.

41. Z. Qianqian, B. Tang and H. Guoxin, J. Hazard. Mater., 2011, 198, 78-86.

42. A. R. Siamaki, A. E. R. S. Khder, V. Abdelsayed, M. S. El-Shall and B. F. Gupton, J. Catal., 2011, 279, 1-11.

43. N. Kovtyukhova, I., P. Ollivier, J., B. Martin, R., T. Mallouk, E., S. Chizhik, A., E. Buzaneva, V. and A. Gorchinskiy, D., Chem. Mater., 1999, 11, 771-778.

44. C. Fu, Y. Kuang, Z. Huang, X. Wang, Y. Yin, J. Chen and H. Zhou, J Solid State Electrochem, 2011, 15, 2581-2585.

45. H. Hassan, M., V. abdelsayed, A. E. R. S. Khder, K. M. AbouZeid, J. Terner, M. Samy El-Shall, S. Al-Resayes, I. and A. A. El-Azhary, J. Mater. Chem., 2009, 19, 3832-3837.

46. D. F. Wang, D. Chen, G. X. Ping, C. Wang, H. Z. Chen and K. Y. Shu, Adv. Mater. Res., 2012, 430-432, 1005-1008.

47. X. Zhou, T. Shi, J. Wu and H. Zhou, Appl. Surf. Sci., 2013, 287, 359-368.

48. Z. Li, B. Gao, G. Z. Chen, R. Mokaya, S. Sotiropoulos and G. Li Puma, Appl. Catal. B: Environ., 2011, 110, 50-57.

49. D. Graf, F. Molitor, K. Ensslin, C. Stampfer, A. Jungen, C. Hierold and L. Wirtz, Nano Lett., 2007, 7, 238-242.

50. M. A. Pimenta, G. Dresselhaus, M. S. Dresselhaus, L. G. Cancado, A. Jorio and R. Saito, Phys. Chem. Chem. Phys., 2007, 9, 1276-1290.

51. C. Xu, J. Wang, L. Wan, J. Lin and X. Wang, J. Mater. Chem., 2011, 21, 10463-10471.

52. C. Casiraghi, S. Pisana, K. S. Novoselov, A. K. Geim and A. C. Ferrari, Appl. Phys. Lett., 2007, 91, -.

53. O. Akhavan, ACS Nano, 2010, 4, 4174-4180.

54. M. Alexander, V. Roumen, S. Koen, V. Alexander, Z. Liang, T. Gustaaf Van, V. Annick and H. Chris Van, Nanotechnology, 2008, 19, 305604.

55. Z. Zhang, W. Yang, X. Zou, F. Xu, X. Wang, B. Zhang and J. Tang, J. Colloid Interf. Sci., 2012, 386, 198-204.

56. W. Zhang, X. Shi, Y. Zhang, W. Gu, B. Li and Y. Xian, J. Mater. Chem. A, 2013, 1, 1745-1753.

57. S. Stankovich, D. A. Dikin, R. D. Piner, K. A. Kohlhaas, A. Kleinhammes, Y. Jia, Y. Wu, S. T. Nguyen and R. S. Ruoff, Carbon, 2007, 45, 1558-1565.

58. T. S. Sreeprasad, S. M. Maliyekkal, K. P. Lisha and T. Pradeep, J. Hazard. Mater., 2011, 186, 921-931.

59. T. N. Lambert, C. A. Chavez, B. Hernandez-Sanchez, P. Lu, N. S. Bell, A. Ambrosini, T. Friedman, T. J. Boyle, D. R. Wheeler and D. L. Huber, J. Phys. Chem C, 2009, 113, 19812-19823.

60. U. Balachandran and N. G. Eror, J. Solid State Chem., 1982, 42, 276-282.

61. K. Zhang, K. C. Kemp and V. Chandra, Mater. Lett., 2012, 81, 127-130.

62. C. Hauf, R. Kniep and G. Pfaff, J. Mater. Sci., 1999, 34, 1287-1292.

63. H. Sheng, H. Ji, W. Ma, C. Chen and J. Zhao, Angewandte Chemie International Edition, 2013, 52, 9686-9690.